Colloid Polym Sci (2004) 282: 854–866
DOI 10.1007/s00396-004-1118-z

ORIGINAL CONTRIBUTION

R. J. Davies
N. E. Zafeiropoulos
K. Schneider
S. V. Roth
M. Burghammer
C. Riekel
J. C. Kotek
M. Stamm

The use of synchrotron X-ray scattering coupled with in situ mechanical testing for studying deformation and structural change in isotactic polypropylene

Received: 27 February 2004
Accepted: 26 March 2004
Published online: 24 April 2004

R. J. Davies · S. V. Roth
M. Burghammer · C. Riekel
European Synchrotron Radiation Facility (ESRF), BP 220, F-38043 Grenoble, France

N. E. Zafeiropoulos (✉)
K. Schneider · M. Stamm
Institut für Polymerforschung Dresden (IPF), Hohe Strasse 6, 01069 Dresden, Germany
E-mail: zafeiropoulos@ipfdd.de

J. C. Kotek
Institute of Macromolecular Chemistry, Academy of Sciences of the Czech Republic, 16206 Prague 6, Czech Republic

Abstract The mechanical behaviour of semi-crystalline polymers is greatly influenced by the properties of the crystalline and the amorphous phases. As a result this topic has been the subject of extensive research. However, to date, a comprehensive relationship between the structure and mechanical properties for semi-crystalline polymers has yet to be established. This present study concerns the commissioning of a novel method for in situ data collection during the deformation of polymers. This involves the combination of three different techniques into a single experiment, namely tensile testing, synchrotron radiation wide angle X-ray scattering, and optical microscopy. For this current investigation, three isotactic polypropylene samples have been studied, produced using different thermal treatments. This enables the influence of thermal treatment on the mechanical properties and crystallographic structure to be assessed. The results indicate that tensile properties are influenced by thermal treatment via the relative fraction of β-phase material in the sample. As the temperature increases at which thermal treatment takes place, iPP ductility decreases due to the greater rigidity of the increasing α-phase content. Differences in crystal strain between the different iPP crystal phases are also observed although the reasons for such differences remain unclear.

Keywords Polypropylene · βiPP · Synchrotron · WAXS · Deformation

Introduction

Isotactic polypropylene (iPP) is a semi-crystalline polymer that has been studied extensively due to its popularity for commercial applications. This can in part be attributed to the relatively low manufacturing cost of iPP and its versatile properties. In particular, the ease of which is it possible to control supermolecular structure by the addition of nucleating agents provides a simple method of obtaining a range of mechanical properties. Thus iPP is currently the polymer with the fastest production and consumption growth [1].

The crystal structure of iPP exists in several different allotropic modifications, all sharing the same threefold helical conformation [2, 3]. The monoclinic α-form (αiPP) is the most stable and is therefore, under standard synthesis and processing, the predominant structure in melt-crystallised iPP [4]. It is characterised by a lenticular lamellae arrangement elongated in the [100] direction of the unit cell [5]. This 'cross-hatched' lamellar morphology exhibits an 80° or 100° branching angle between the tangential and radial lamellae [2, 6, 7].

The β-form (βiPP) was first identified by Keith et al. and is thermodynamically and mechanically less stable than the α-form [2, 8]. This results in a significantly

lower melting temperature [1, 9, 10]. Crystallisation of the β-form is also significantly faster than that of the α-form [2, 9, 11]. The β-form of iPP exhibits a pseudo-hexagonal structure and is thought to exist in a high degree of disorder [12]. Spherulites of βiPP differ significantly from those of αiPP as they exhibit an exclusively radial lamellar arrangement [6, 7].

The γ-form of iPP generally only occurs during slow crystallisation at high-pressure or during shear flow [2, 7, 13, 14]. Under standard iPP processing conditions it is present only in small traces [13]. It exhibits an orthorhombic structure and is characterised by a high degree of molecular orientation [7, 14].

Although crystallisation of the αiPP is preferred (due to it being thermodynamically more stable), crystallisation to the β-modification may be encouraged under certain conditions. Such conditions include directional crystallisation in a temperature gradient or from melts subjected to shear forces [10, 11]. Whilst these methods can produce iPP with a significant β-phase content, usually the α-phase is also present in non-negligible quantities [12]. Thus, iPP produced using these methods is not well suited for exclusive study of the β-phase. It is however possible to produce βiPP of greater purity with the inclusion of nucleation agents in the melt [1, 7, 11, 15, 16]. Thus the production of iPP with nucleating agents provides a convenient basis for the study of βiPP [7].

Along with the variations in crystallographic structure between the different iPP forms, significant differences in their mechanical properties have also been reported [5, 7, 11]. An increase of the β-phase content is found to decrease both the Young's modulus and the yield stress whilst increasing the elongation to break [7, 11]. This has been explained by the greater rigidity of the α-phase lamellar structure where there exists a radial and tangential lamellae arrangement [7]. An SEM observation of direct spherulite deformation also reports that the lamellae in β-spherulites are able to slide over one another (crystalline plastic slip) [17]. This was found to occur during large deformations and results in a lamellar structure oriented to the stress direction [17]. It is thought that this sliding behaviour is made possible by the mobility of the interlamellae amorphous zones [17]. This may also explain the higher elongation to break of specimens with higher β-phase content as the branched structure of the α-phase promotes breakage within the spherulites at lower strain levels [17].

The tensile properties of iPP are reported to be relatively insensitive to changes in the β-phase content [7]. Therefore, increasing the β-phase content only slowly reduces Young's modulus and yield stress [7]. It has been previously suggested that individual spherulites may simultaneously include both an α- and β-phase [7, 12]. The gradual replacement of the α- phase during heat-treatment would explain this insensitivity [7].

As well as the differences in mechanical properties between the different forms of iPP, an improvement in the tensile properties of βiPP is also observed during mechanical loading [18]. This is thought to arise from modification of the βiPP crystal structure during deformation [18]. The use of WAXS allows these deformation-induced changes to be investigated. Such studies generally involve performing WAXS on pre-deformed iPP specimens [1, 5, 19, 20]. It has been demonstrated for βiPP that the metastable β-phase can be readily transformed into α-phase during solid-state drawing at elevated temperatures [1]. Under such conditions the β-phase fraction is found to decrease with increasing draw ratio; however, overall crystallinity remains unchanged [1]. In the necked region, both the α- and β-phases show an improvement in molecular orientation along the draw direction [1].

A mechanically-induced β- to α-phase transition has also been reported during deformation at room temperature [5, 18, 19, 20]. During such experiments the phase transition is observed to be more extensive in the deformed neck region of the specimen [5]. A synchrotron study by Riekel and Karger-Kocsis used a micro-focus beam to assess the degree of phase transformation as a function of distance (that is from the undeformed region of the sample to the deformed region) along a pre-deformed specimen [19]. The α/β ratio was reported to increase as a function of overall strain [19]. The same study also reported an almost pure conformationally disordered (condis) phase (co-iPP) at the edge of the deformed region [19]. This phase was found to be highly oriented and to exhibit a fibre-diffraction type WAXS pattern [19].

The transition during deformation of iPP from the β- to α-phase has also been considered by Li and Cheung [20]. They proposed that the β-phase of iPP is mechanically stable to the yield point and transforms to the α-phase only during necking [20]. Stress-induced melting of the pre-existing crystallites must therefore occur [20]. This melting process is localised in areas where stresses are particularly high rather than occurring throughout the whole neck region [20]. This hypothesis is confirmed using SEM where localised melting is observed in β-phase lamellae that are parallel to the stretching direction [21, 22].

This present study reports the initial findings of an investigation into the influence of mechanical deformation on the crystallographic structure of βiPP. Several varieties of βiPP are investigated which were produced using a variety of thermal treatments. Thus the effect of variations in the crystallisation regime can be assessed. Such an approach may help elucidate the complex relationships between the microstructure of βiPP and its macroscopic properties.

The deformation of specimens in this study has been carried out in situ with simultaneous synchrotron WAXS.

Whilst several previous synchrotron studies of iPP have also been performed in situ, these have been concerned with in situ crystallisation and melting behaviour [4, 16, 23, 24, 25, 26, 27]. A previous synchrotron study investigating deformation-induced phase transitions was limited to a pre-deformed iPP sample [19].

The use of a synchrotron radiation source for this experiment offers several advantages over standard laboratory apparatus. The higher brilliance of the source permits the generation of diffraction patterns at a higher frequency than is possible using a laboratory diffractometer. This is of particular importance for time-resolved studies and allows samples to be tested dynamically. The use of a synchrotron source also allows the beam to be focussed to small spot-sizes. For this experiment diffraction patterns were generated using a micro-focus synchrotron beam. This minimises averaging by reducing the volume of material from which diffraction takes place.

Experimental

Materials

The samples were prepared by punching discs of material (∅ 6.5 mm) from a thermopressed film of 0.6 mm thickness. Afterwards, samples were subjected to a range of thermal treatments (145, 125, 120 °C, for 1 h isothermal crystallisation) with the use of DSC Q1000 (TA Instruments) apparatus. The discs were then machined with a CNC milling machine to produce the geometry shown in Fig. 1. Isotactic polypropylene (Novolen 1100 N, BASF AG) was used as starting material throughout the present study. This polymer was modified by a selective β-nucleation agent (NJ-Star NU-100, Rika International, Manchester, UK) based on N',N′-dicyclohexylnaphthalene-2,6-dicarboxamide, which was added into the polypropylene in the form of a master batch. The concentration of the nucleating agent was 0.03 wt%. This has to been found to be the critical concentration for high β-phase content in a previous study [11].

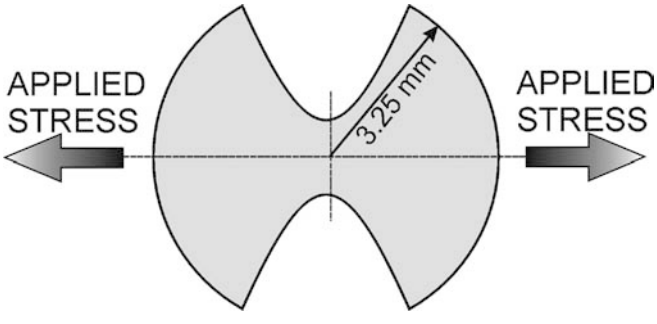

Fig. 1 Tensile specimen sample geometry

In situ tensile testing

Tensile tests were performed on a custom-made deformation rig, with measurements taken in situ during X-ray scattering. The strain rate applied on all samples was 0.3%/s. The rig consists of two mounting grips, on which the sample is mounted and fixed in position using screws. The grips move in opposing directions at constant speed, and are powered through a single motor. This setup allows observation of the same point on the sample during the whole test period. A load cell is fixed to one sample grip, and the displacement of the grips measured using an electrical inductor (L). All the components of the rig are interfaced with a PC with a data recording frequency of 5 s for all experiments. The measurements from the rig enable nominal force vs displacement plots to be produced. A camera was also employed to record images of the sample in situ during deformation. An on-axis mirror between the final aperture and sample enabled images to be captured along the beam axis direction. Images from the camera were also recorded at 5-s intervals during all experiments. A photograph of the deformation rig in situ is shown in Fig. 2.

Synchrotron WAXS

Data collection WAXS of all samples was carried out at the European Synchrotron Radiation Facility (ESRF) on the micro-focus beamline (ID13). The beamline was configured with a Kirkpatrick-Baez (KB) type mirror and collimated using a piezo-based block collimation system to provide an on-sample beam spot-size of approximately 5 μm. A radiation of wavelength 0.098 nm was used during all experiments. The beam position on the sample was fixed at the centre of the deformation region during all tests, approximately midway between the mounting grips. Thus variations in beam position on the sample arise only through sample extension during testing.

Samples were deformed in situ using the custom-built deformation rig attached directly to the beamline positioning stage. For data collection a MARCCD detector was used with an average pixel size of 64.45×64.45 μm^2. Prior to the start of the experiment diffraction patterns were obtained from corundum powder. The reflection positions were then used in conjunction with literature values to calculate the sample-to-detector distance. This was found to be 159 mm. The powder diffraction rings were also used to determine the beam centre position and calibrate detector tilt and rotation using the Fit2D software application [28, 29]. Prior to deforming each sample, a background diffraction pattern was recorded. This could then be subtracted from sample diffraction

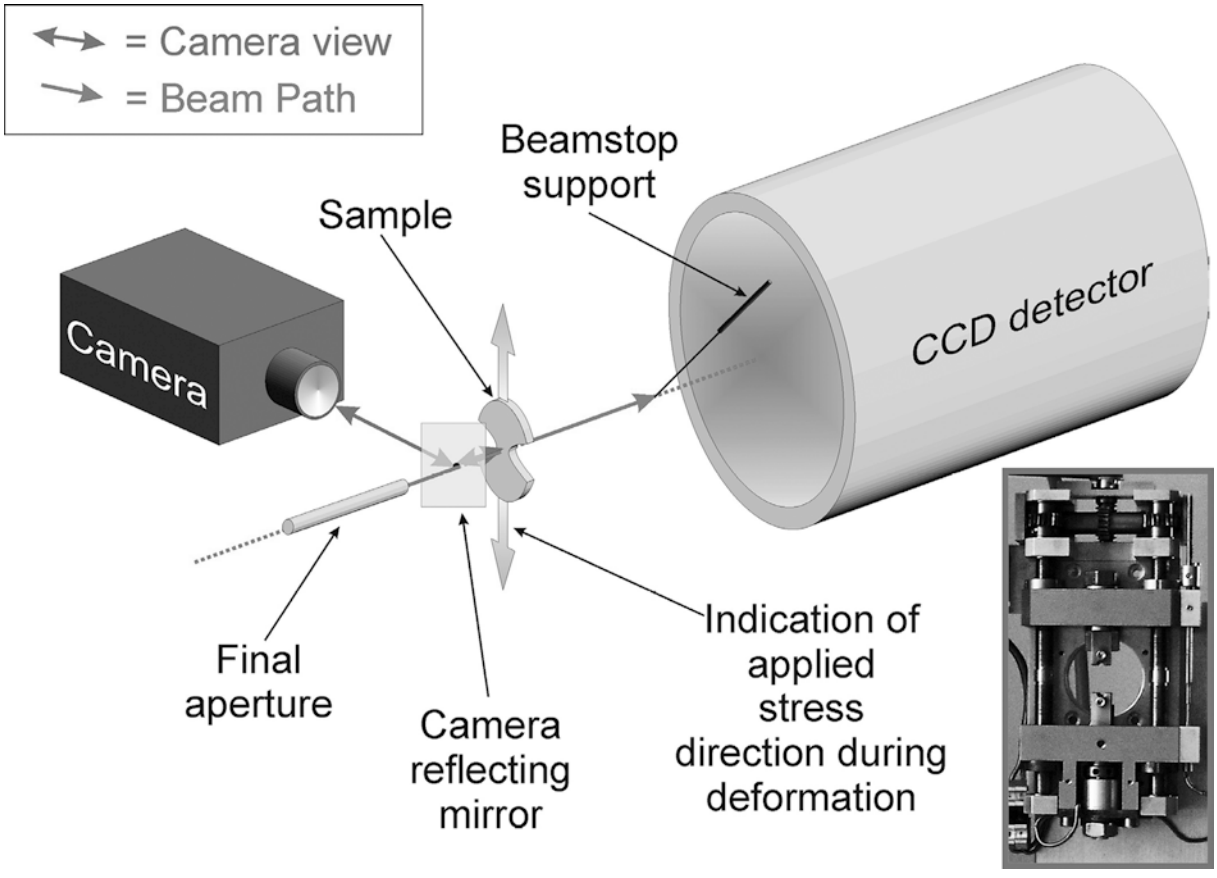

Fig. 2 Schematic view of experimental setup and (*inset*) photograph showing sample deformation rig (note schematic drawing is not to scale)

patterns prior to analysis. This helps to eliminate beam-stop or aperture artefacts and reduces the influence of air scattering intensity.

Diffraction patterns were generated at 11-s intervals using an exposure time of 1 s. Sample deformation continued in each case until either the material in the beam was insufficient to generate diffraction data or sample failure occurred. Figure 3 shows typical diffraction patterns taken from βiPP samples thermally treated at 120 and 145 °C. Both diffraction patterns are shown from samples prior to deformation.

Data treatment Treatment of the WAXS data was performed using a combination of the Fit2D software application and a custom-written batch peak-fitting program. Fit2D was used to perform background subtraction, spatially correct the diffraction patterns and calculate integrations of reflection intensity. The batch peak-fitting software was used to fit the resulting intensity profiles using standard functions.

For analysis of radial profiles, the diffraction patterns were azimuthally integrated over a 300° range. Although a complete 360° integration is preferred, the shadow created by the beam-stop makes this approach unsuitable. By integrating around nearly the entire powder ring, any variations or inaccuracies in the beam centre position are eliminated. Additionally, this provides the greatest possible intensity profile, reducing possible fitting errors and eliminating any variations arising through crystallite orientation changes. The integrated reflections were fitted using Lorentzian functions to determine the position of each maxima. Lorentzian functions were chosen as they were found to provide an accurate fit to the data. A background was also fitted comprising of a single Lorentzian function to fit the amorphous halo and a further fixed linear function. Figure 4 shows a typical βiPP profile to demonstrate reflection fitting, in this case taken from the sample thermally treated at 145 °C. To calculate crystal lattice spacings from the determined reflection positions the Bragg equation was used. In order to determine the relative β-phase content of each sample, the method proposed by Jones et al. has been employed [30]. The β-phase fraction (K_β) is given by Eq. (1):

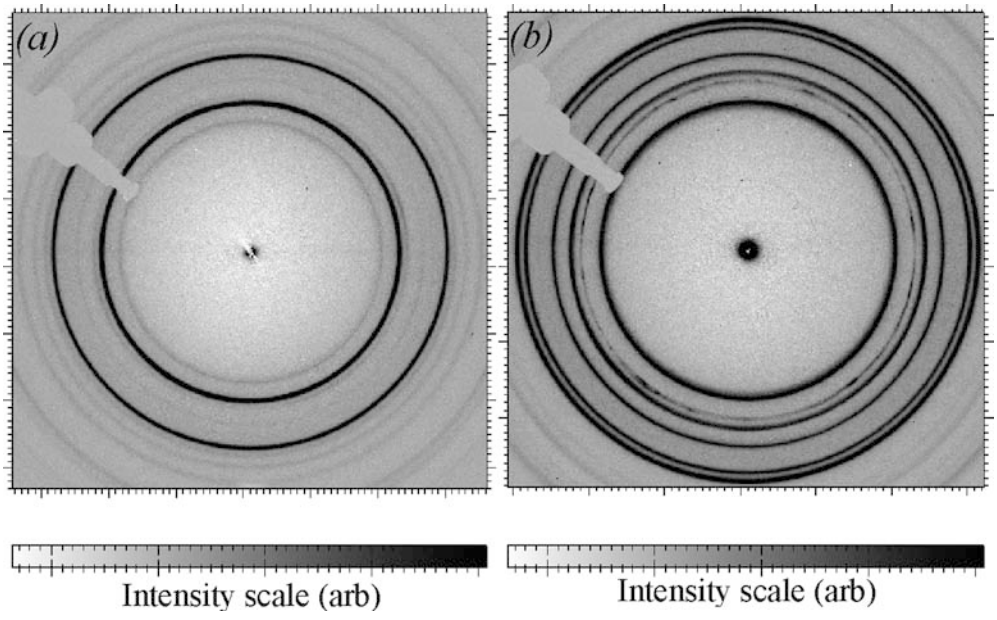

Fig. 3a,b WAXS patterns of βiPP samples thermally treated at: **a** 120 °C; **b** 145 °C

$$K_\beta = \frac{I_{(2\bar{1}0)\beta}}{I_{(2\bar{1}0)\beta} + I_{(110)\alpha} + I_{(040)\alpha} + I_{(130)\alpha}} \quad (1)$$

where $I_{(210)\beta}$ is the integrated intensity of the $(2\bar{1}0)$ reflection, and $I_{(110)\alpha}$, $I_{(040)\alpha}$ and $I_{(130)\alpha}$ are the integrated intensities of the (110), (040) and (130) reflections respectively. The applicability of this method is confirmed by its extensive use in other studies of βiPP [8, 10, 11, 23, 25, 31]. For an estimation of the crystallinity index (X_c) the apparent crystalline fraction may be calculated. In this case the fraction of crystalline components within the 2θ range of 6–16° is calculated by Eq. (2) [10, 11]:

$$X_c = \frac{I_c}{I_c + I_a} \quad (2)$$

where I_c and I_a are the integral intensities of the one-dimensionally fitted crystalline peaks and amorphous halo respectively.

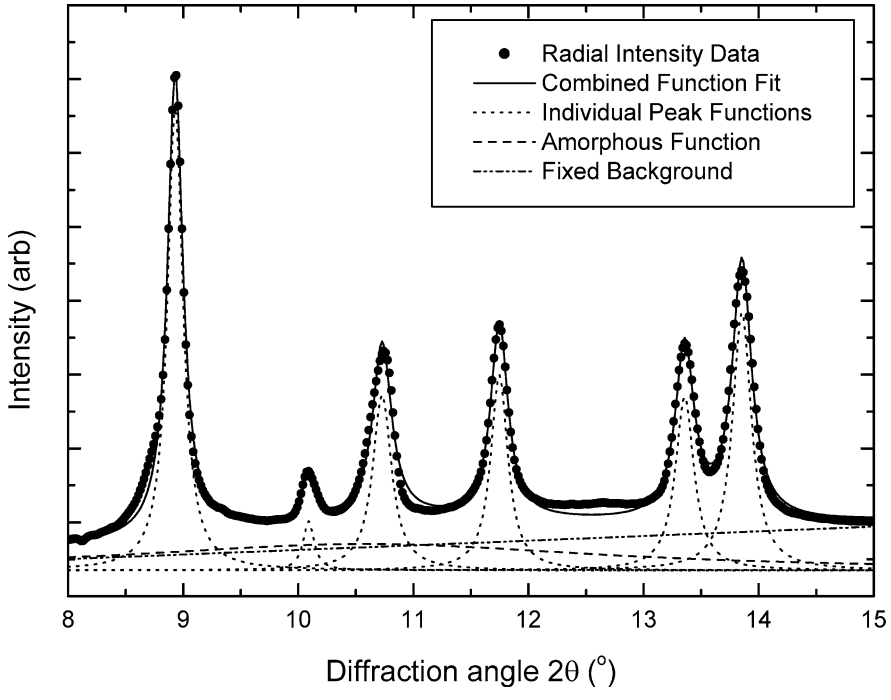

Fig. 4 Example of diffraction profile fitting using Lorentzian functions (sample is βiPP thermally treated at 145 °C)

Results and discussion

In situ camera images

Figure 5 shows images captured by the in situ camera of the three samples under study. Note that the darker region in the bottom right hand corner of each sample is a shadow created by the lighting arrangement. All three images were captured at the end of the experiments, therefore showing fully deformed material. There is a significant difference between the sample thermally treated at 145 °C compared to the other samples. In this case the specimen maintains the glassy appearance visible prior to deformation whilst exhibiting a network of cracks close to the failure region. This suggests that no yielding occurred in this sample prior to failure. Both the 120 and 125 °C samples show significant yielding with the specimens becoming opaque and highly extended. This suggests these samples are ductile with significant plastic deformation occurring prior to failure.

Failure of the sample thermally treated at 145 °C is indicative of brittle fracture with a large fracture rapidly occurring across the entire sample width. The 120 °C sample shows a ductile fracture pattern with a crack appearing near one edge of the specimen corresponding to the region of maximum stress concentration. This crack then propagates across the yielded sample with increasing strain. The mechanism of fracture is very similar to the one described by Bessell et al. [32], whereby a series of microcracks nucleate intraspherulitically and then coalesce to form a crack that propagates in a ductile manner. The 125 °C sample shows a fracture behaviour quite different to that of the 120 °C sample. In this case a critical flaw appears in the centre of the specimen which propagates outwards with increasing strain. The mode of failure is similar to the mechanism termed as 'cup-and-cone fractures' [33]. Heterogeneities, such as inclusions and second-phase particles, result in the nucleation of holes that grow by plastic deformation in the non-uniform stress field of the neck (usually in the centre of the neck). The plastic cavities then grow due to the additional tensile stresses normal to the tensile axis generated by the neck geometry. In the case of semi-crystalline polymers it has been previously shown that cavitation occurs during tensile testing [34]. It is possible that these cavitations become critical flaws that either grow plastically, coalescing to form ductile cracks in the centre of the neck or edges of the sample, or they coalesce rapidly to form a brittle crack that causes a swift catastrophic failure. However, which mechanism operates under which conditions in the case of iPP is still unclear at this point. The possibility of accelerated failure through localised beam heating cannot be excluded, but seems unlikely considering the small beam size used in this study.

In situ tensile results

Figure 6 shows a nominal force vs strain plot for the three different βiPP samples. Nominal force has been determined from the voltage output of the force sensor whilst strain has been calculated from the movement of two marked points on the video images with

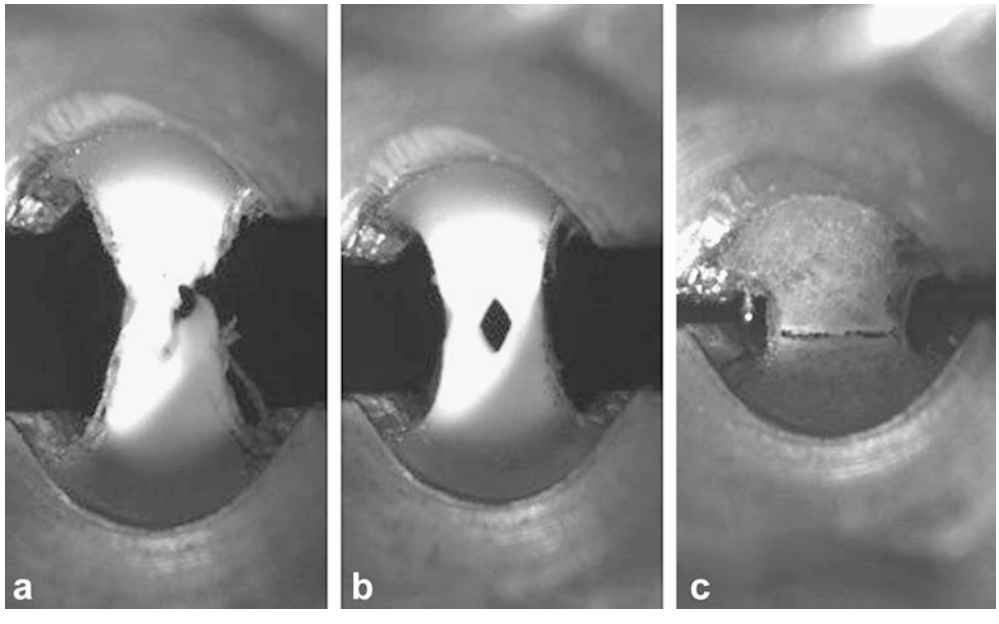

Fig. 5a–c In situ camera images of deformed βiPP samples thermally treated at: **a** 120 °C; **b** 125 °C; **c** 145 °C

deformation. This value can be taken as strain in the middle of the specimen (approximately in the locality of the beam).

In the low-strain region (up to around 12%) all samples show a linear relationship between nominal force and strain. This initial deformation is predominantly elastic in nature with no significant differences in the results obtained between different samples. This suggests that thermal treatment has little influence on tensile behaviour in the low strain region when deformation is occurring under an elastic regime.

Failure of the sample thermally treated at 145 °C occurs comparatively rapidly at approximately 12% strain. The fact that the tensile plot of this sample is approximately linear until failure indicates that only negligible plastic deformation occurs and sample failure is through brittle fracture. This is consistent with observations from the in situ camera images (Fig. 5). Deformation of the other βiPP samples continues to much higher strain levels before failure. In the samples thermally treated at 120 and 125 °C, nominal force becomes relatively constant at strain levels greater than 12%. This indicates that the yield point for all βiPP samples occurs at around 12% strain. Thus, the samples thermally treated at lower temperatures are ductile in nature with deformation leading to significant yielding. This conclusion also correlates well with the images obtained from the in situ camera (Fig. 5).

Nominal force begins to decrease with increasing strain above 130% and 100% strain for the samples thermally treated at 120 and 125 °C respectively. The time at which this decrease occurs corresponds to the appearance of the fracture mechanisms observed on the in situ camera images. It is evident from these results that thermal treatment has a significant influence on material tensile properties. The higher the thermal treatment temperature, the less yielding occurs during deformation. Thus, increasing temperature decreases the ductility of βiPP. It is also worth noting that the observation in previous studies that the tensile properties of βiPP improve during mechanical loading is not evident from the results obtained in this study (Fig. 6) [18]. Such an improvement has previously been attributed to a mechanically-induced phase transition of β-phase iPP to the α-phase modification. One possible explanation for the absence of this effect is that premature sample failure may have occurred. The elongation to break of βiPP reported in previous studies is much greater than that achieved in this study, with deformation continuing to well above 200% strain [11, 18, 20].

Also shown in Fig. 6 are the diffraction limits for each βiPP sample. These limits reflect the fact that diffraction data could not always be collected until sample failure. Thus the diffraction limits indicate the point at which further data collection was not possible for each sample. This situation arises due to either no sample material being in the beam path (when a fracture appears for example) or because sample gauge volume becomes too low to generate meaningful diffraction data.

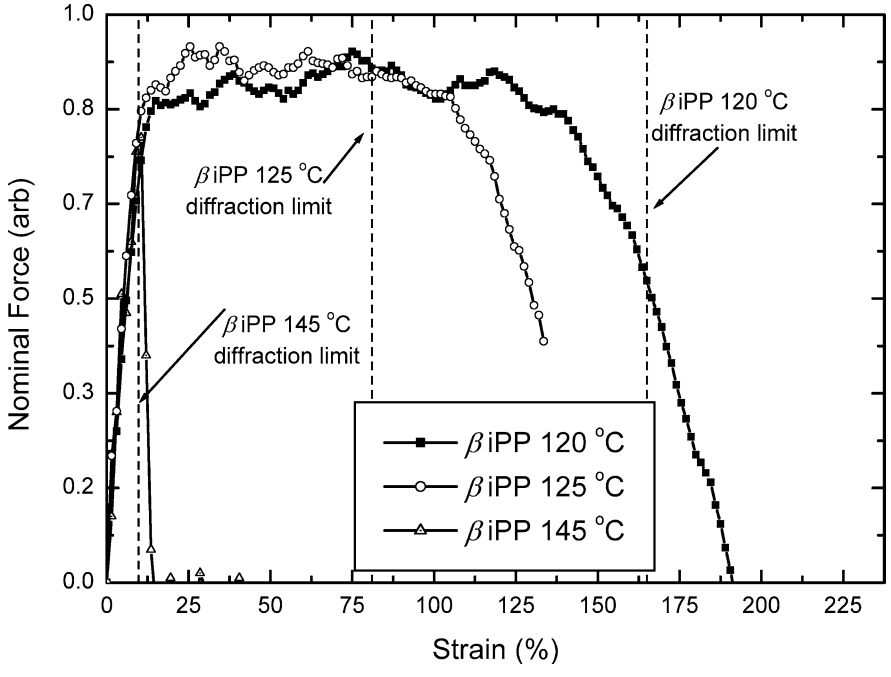

Fig. 6 Nominal force vs strain curves from in situ deformation rig measurements

Synchrotron WAXS

Undeformed samples

Figure 7 shows WAXS radial intensity profiles of all three undeformed βiPP samples for direct comparison. The intensity values have been offset for clarity and the reflections indexed in accordance with several previous studies [1, 2, 12, 19, 26, 31]. All samples show prominent reflections around 0.55 nm (reflection $(2\bar{1}0)$) and 0.42 nm (reflection $(2\bar{1}1)$, characteristic of the iPP β-phase [1, 6, 19]. The sample thermally treated at 145 °C also shows significant scattering intensity for reflections associated with the α-phase. By contrast, α-phase scattering is almost completely absent from the samples thermally treated at 120 and 125 °C. Therefore with increasing thermal treatment temperature, the β-phase content decreases and the fraction of α-phase increases. This relationship is confirmed by calculating the β-phase fraction using Eq. (1). The results of this calculation are collected in Table 1. Error values have been estimated based upon fitting uncertainty and variations between consecutive data fits. The fact that the error is greater for samples with a higher β-phase content reflects the difficulty in fitting α-phase reflections with a significantly lower intensity. The relationship between crystallisation regime and β-phase content is well documented [1, 11, 23, 25]. The maximum radial growth rate of βiPP spherulites occurs during crystallisation at 123 °C [7]. This accounts for the higher β-phase fraction in the samples crystallised at 120 and 125 °C in this study. Furthermore, the formation of β-phase crystals is not-favoured in thermal regimes much above 140 °C, thus formation of the thermodynamically more stable α-phase crystals takes place [35]. It is therefore of no surprise that the sample thermally treated at 145 °C predominantly contains α-phase crystals.

Values for the initial crystallinity index of the βiPP samples have been calculated according to Eq. (2) with the results collected in Table 1. The error values for crystallinity index are estimated based upon the fitting uncertainty; however it should be noted that there may be other larger errors due to differences in amorphous material between samples. A more accurate calculation of crystallinity is precluded by the difficulty in obtaining purely amorphous iPP material. The values for crystallinity index are similar between all samples, being around 60% (within experimental error). Both β-phase fraction and crystallinity index are also similar to those observed in a previous study for the samples thermally treated at 120 and 125 °C [11].

The WAXS results can also be used to explain the variations in tensile behaviour observed in Fig. 6 and in the in situ images shown in Fig. 5. The fact that increasing β-phase content increases the elongation to break has been previously attributed to the greater rigidity of the α-phase lamellar structure [7]. For large deformations the lamellae in β-phase spherulites are subject to crystalline plastic slip, as reported from SEM observations [17]. This yielding behaviour is precluded in α-phase material. Thus the elastic deformation and brittle fracture of the βiPP sample thermally treated at

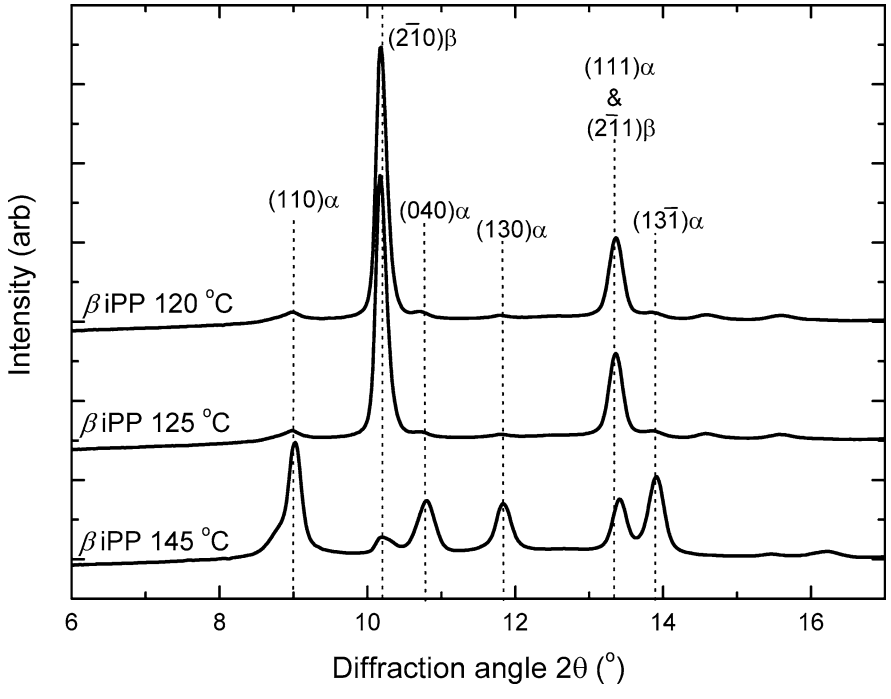

Fig. 7 Indexed radial intensity profiles of βiPP samples

Table 1 Variation of β-phase fraction and apparent crystallinity between specimens

	βiPP 120 °C	βiPP 125 °C	βiPP 145 °C
β-Phase fraction (K_β)	85.8% (±5.5)	86.0% (±5.6)	7.9% (±1.9)
Crystallinity index (X_c)	55.6% (±4.7)	60.0% (±6.5)	61.9% (±4.8)

145 °C may be attributed to its predominantly α-phase content. In addition to this, it has also been shown that samples with larger spherulites fail in a brittle manner [17]. Extensive crazi and void formation takes place at spherulitic boundaries inside which, low molecular weight material and other impurities are concentrated. These therefore serve to act as stress concentration points [17, 36].

It is also clear from Fig. 6 that the sample thermally treated at 120 °C has a higher elongation to break than the 125 °C sample. Whilst this could be adequately explained by a different β-phase fraction between the two samples, the β-phase fraction is in fact similar. It is also interesting to note that the crystallinity index values appear to be the same between these two samples (Table 1). The differences in elongation to break shown in Fig. 6 are therefore probably related to the variations in fracture behaviour observed in Fig. 5. There is no explanation at this point as to why these two quite similar samples exhibit such differences in their mechanisms of fracture. However, there are probably other factors which would also be influential such as cavitation for example.

Also noteworthy in Fig. 7 is that the sample thermally treated at 145 °C shows a significant degree of asymmetry from scattering associated with the (110) reflection. This can be attributed to heterogeneity in the specimen, specifically variations in the distribution of crystalline regions along the beam axis direction. Figure 3 also shows that scattering associated with the $(2\bar{1}0)$ reflection is anisotropic for the same sample. This may suggests the existence of local texturing in β-phase crystalline regions. The significance of the anisotropy is difficult to gauge considering the small sample volume irradiated by the micro-focus beam.

During deformation

Figure 8 shows the variation in β-phase fraction with deformation. The sample thermally treated at 120 °C exhibits the greatest decrease in β-phase fraction of approximately 15% in total. The specimen thermally treated at 125 °C also shows a significant decrease at approximately 60% strain, although the β-phase fraction appears to increase again in the final two data points in the series. The 145 °C sample shows no significant reduction in β-phase fraction with increasing strain; however, only four measurements were obtained prior to sample failure.

These results are consistent with the findings of previous studies which report that deformation of βiPP may induce a β- to α-phase transition [5, 19, 20]. The fact that the β-phase of iPP is mechanically stable to the yield point explains the absence of a significant decrease in

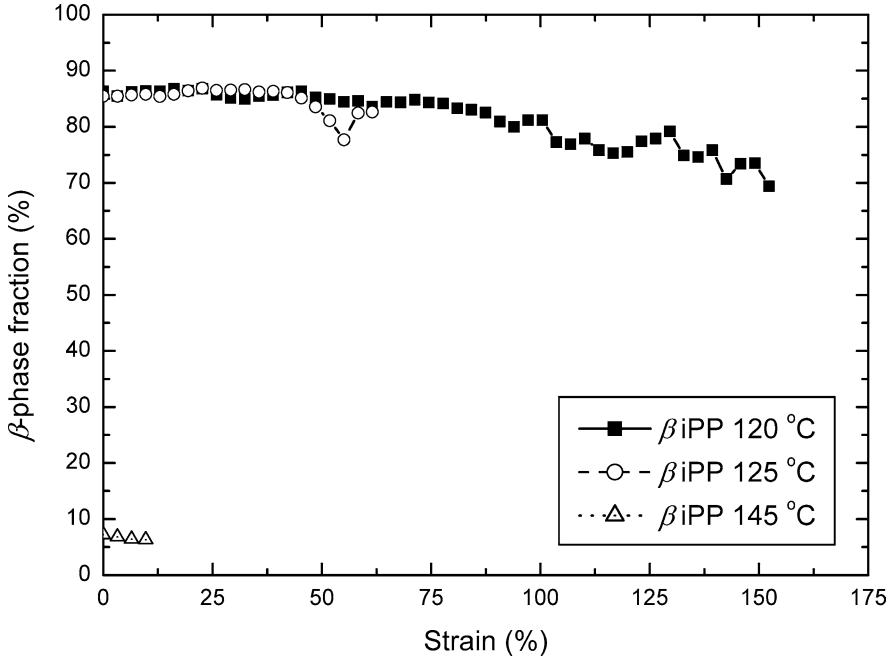

Fig. 8 Variation in β-phase fraction with deformation between βiPP samples

β-phase fraction in the sample thermally treated at 145 °C [20]. Whilst these results are consistent with those of previous studies on samples deformed ex situ the magnitude of this effect is much less than previously reported [5, 19, 20]. A previous study by Li and Cheung [20] measured the change in β-phase fraction in a pre-deformed βiPP sample using DSC measurements [20]. The β-phase fraction was found to decrease by approximately 35% at 230% elongation [20]. Conversely the α-phase content was found to increase 27% in the same specimen [20]. The low magnitude of the β- to α-phase transition reported in this study may be attributed to the lower strain achieved during testing. Diffraction data could not be obtained at high sample strain because of the occurrence of fractures in the locality of the beam position and the reduction in scattering intensity due to the decreasing sample volume. The greatest extension achieved during this study was for the sample thermally treated at 120 °C which attained 165% strain. This is still significantly lower than the 230% elongation reported by Li and Cheung [20]. It is also worth pointing out that an accurate determination of the β-phase fraction is more complex for samples with a higher β-phase content due to the lower scattering intensity from α-phase reflections. This favours the use of samples with lower β-phase fractions for studying β- to α-phase transitions, such as those used by Li and Cheung [20].

The full width at half maximum (FWHM) of WAXS reflections may be related to crystallite size, sample heterogeneities (in the beam axis direction) or distributions in lattice distortion. In the case of deformation at room temperature, such variations may be considered as indicating the degree of homology in the stress distribution within the material. Thus a range of stresses acting upon different crystallites results in a distribution in lattice spacing, which corresponds to the reflection FWHM. By monitoring the change in FWHM with increasing strain, it is possible to determine whether macroscopic stress leads to a more or less homologous microscopic stress distribution within the crystal structure. Figure 9 shows the percentage change in FWHM with strain for the $(2\bar{1}0)$ reflection of the different βiPP samples. The overall uncertainty of the calculation comes form the fit and in our case it was always less than 2.4% of the calculated value. As this reflection is associated with the β-phase, the FWHM can therefore be regarded as a measure of the degree of homology in the stress distribution within β-phase material. At low strain levels (up to the yield point), the samples thermally treated at 120 and 125 °C show a similar increase in FWHM with increasing strain. The 145 °C sample shows a much greater increase in FWHM that the other samples within this strain range. This indicates a greater range of lattice distortion in the 145 °C sample which can be attributed to the onset of sample failure. As localised failure begins to occur, a re-distribution of stresses takes place within the material. This results in a greater distribution in lattice distortion as some regions may be highly stressed, whilst those in the failure region will be under comparatively little stress.

If the samples thermally treated at 120 and 125 °C are again considered, both show a region after the yield point of no change in FWHM with increasing strain. This suggests that plastic deformation within the material occurs relatively homogeneously during yielding. The onset of failure in both these samples is again accompanied by an increase in FWHM for the $(2\bar{1}0)$ reflection. The fact that this increase is of a much greater magnitude than that observed in the 145 °C sample may be due to the comparatively lower rigidity of the β-phase compared to the predominantly α-phase 145 °C sample. In addition, the mode of failure for these two samples indicate a large amount of plastic deformation taking place. It is well known that under plastic deformation stress is distributed in a highly inhomogeneous mode [37]. Thus, the abrupt increase of the FWHM may also be caused due to this high stress inhomogeneity.

Figures 9 and 10 show the variation in crystal strain calculated from changes in lattice spacing in the low tensile strain range ($< 40\%$). Once again, also here the error comes from the uncertainties due to the fitting, and always the error was les than 2.3%. At such low strain levels a deformation-induced improvement in crystallite orientation is negligible as it is only observed during relatively extensive yielding in iPP [1, 19]. Investigations of crystal strain within the low strain range therefore preclude differences in crystallite orientations between samples from influencing the results. In Fig. 10 crystal strain is calculated from the (110) reflection which corresponds to scattering from the α-phase. Conversely, in Fig. 11 crystal strain is calculated from the $(2\bar{1}0)$ reflection which corresponds to scattering from the β-phase The failure point of the sample thermally treated at 145 °C is indicated in Fig. 10 for clarity due to the close proximity of the other data series. It is worth noting that a direct comparison of crystal strain between the different crystal planes is somewhat misleading due to the different unit cell structures of the α- and β-phases of iPP. However, relative comparisons between different samples in both Figs. 9 and 10 are still valid.

If the region prior to yielding is first considered, it is immediately apparent that changes in crystal lattice spacing for the (110) reflection of the α-phase are consistent between all βiPP samples. Thus increasing tensile strain results in similar levels of crystallographic deformation in α-phase material independent of thermal history. This is contrasted by the crystal strain results calculated from the $(2\bar{1}0)$ reflection shown in Fig. 11. In this case whilst the samples thermally treated at 120 and 125 °C both show a similar result, the 145 °C sample exhibits a different behaviour. The rate of crystal strain

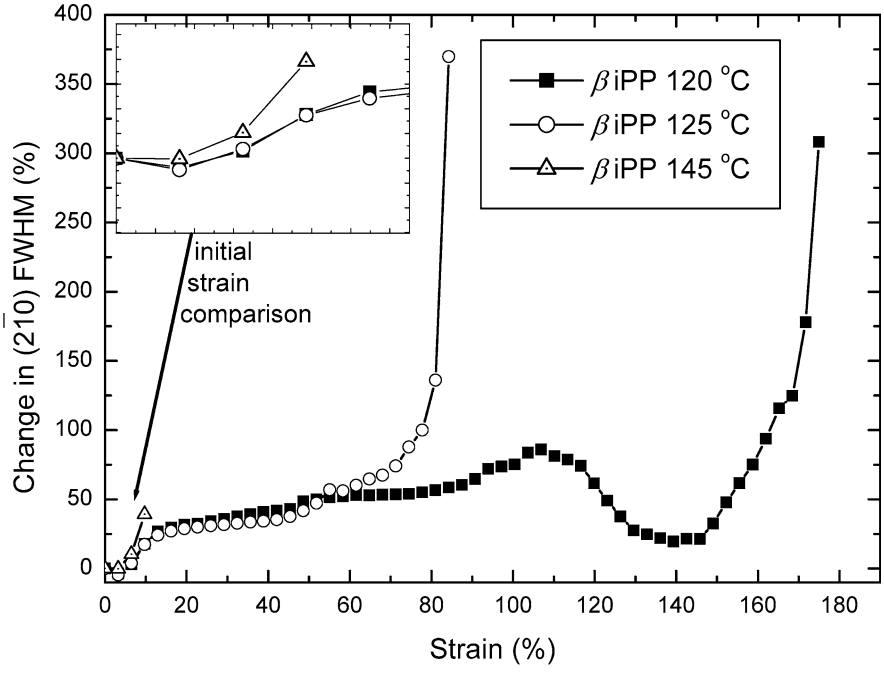

Fig. 9 Percentage change during deformation in FWHM of the (2$\bar{1}$0) reflection fit

increase with increasing tensile strain is greater for the 145 °C sample. The fact that this difference is only evident in the β-phase reflection and not also in the α-phase reflection is particularly interesting. One possible explanation for this may be that the higher content of the rigid α-phase in this sample acts in such a way as to concentrate stress in the dispersed β-phase regions. Although such a hypothesis seems reasonable, without further analysis this conclusion remains purely speculative.

Conclusions

A novel method combining the three different techniques of tensile testing, synchrotron radiation WAXS,

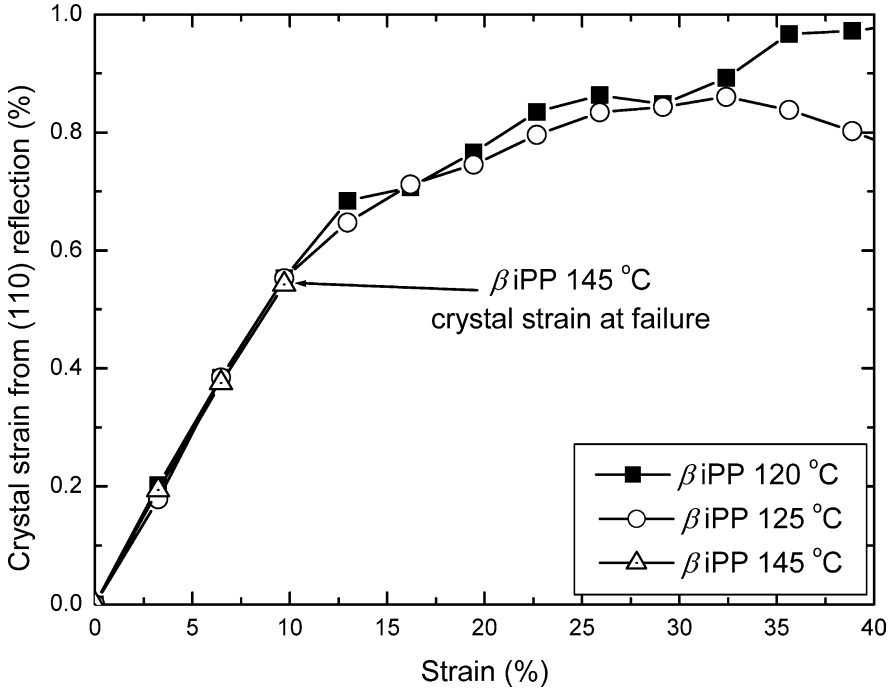

Fig. 10 Variation in crystal strain calculated from the (110) reflection in the low tensile strain region

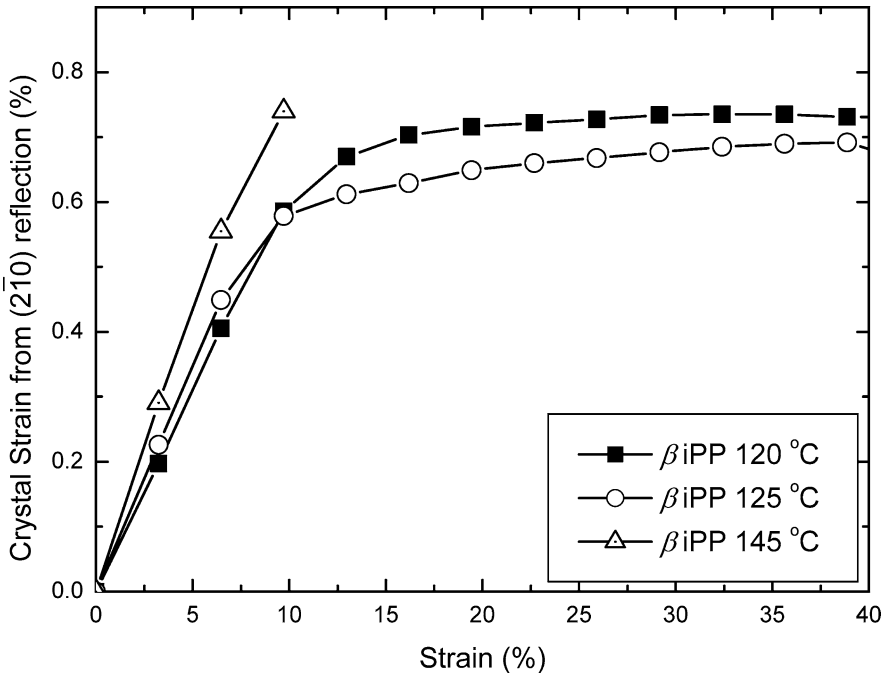

Fig. 11 Variation in crystal strain calculated from the (2$\bar{1}$0) reflection in the low tensile strain region

and optical microscopy has been successfully commissioned to study deformation mechanisms in three different grades of βiPP. The results indicate that although the three different samples have statistically the same apparent crystallinity, the β-phase content varies with β-phase fraction decreasing with increasing temperature during thermal treatment. Additionally, the three samples also appear to exhibit quite different modes of failure.

The determination of FWHM from the (2$\bar{1}$0) reflection associated with the β-phase crystal planes indicates a high level of inhomogeneity in the stress distribution. This is especially apparent approaching sample failure. This result is consistent between samples, irrespective of the thermal treatment conditions. In addition, the β-phase content is found to decrease during the application of tensile strain. This effect is noted to be of a somewhat lower magnitude than previously reported in literature, presumably due to the samples lower elongation to break. A correlation is observed between the β-phase content and yielding during deformation due in part to differences in crystal phase rigidity. Thus, the higher the thermal treatment temperature, the greater the fraction of α-phase material and the more brittle the sample during testing. However, it also appears that the deformation behaviour of iPP does not exclusively depend upon the different crystal phases. Other factors are also thought to be significant such as spherulitic size, and lamellar arrangement. There is currently ongoing work using synchrotron radiation SAXS with in situ tensile testing in order to shed more light on these complex relationships.

Acknowledgements The authors would like to thank the ESRF for beamtime. This project was undertaken as part of a long-term proposal (SC-1099). We would also like to thank Dr Y.-F. Men and Mr M. Amici for assisting with the experiments, and Ms L. Häuβler for preparing the samples at the DSC.

References

1. Ščudla J, Raab M, Eichhorn K-J, Strachota A (2003) Formation and transformation of hierarchical structure of β-nucleated polypropylene characterized by X-ray diffraction, differential scanning calorimetry and scanning electron microscopy. Polymer 44:4655
2. Lotz B, Wittmann JC, Lovinger AJ (1996) Structure and morphology of poly(propylenes): a molecular analysis. Polymer 37:4979
3. Naiki M, Kikkawa T, Endo Y, Nozaki K, Yamamoto T, Hara T (2000) Crystal ordering of α phase isotactic polypropylene. Polymer 42:5471
4. Vleeshouwers S (1997) Simultaneous in-situ WAXS/SAXS and d.s.c. study of the recrystallization and melting behaviour of the α and β form of iPP. Polymer 38:3213

5. Grein C, Plummer CJG, Kausch H-H, Germain Y, Béguelin P (2002) Influence of β nucleation on the mechanical properties of isotactic polypropylene and rubber modified isotactic polypropylene. Polymer 43:3279
6. Norton DR, Keller A (1985) The spherulitic and lamellar morphology of melt-crystallized isotactic polypropylene. Polymer 26:704
7. Tordjeman P, Robert C, Martin G, Gerard P (2001) The effect of α, β crystalline structure on the mechanical properties of polypropylene. Eur Phys J E 4:459
8. Keith HD, Padden FJ Jr, Walter NM, Wyckoff HW (1959) Evidence for a second crystal form of polypropylene. J Appl Phys 30:1485
9. Lotz B (1998) α and β phases of isotactic polypropylene: a case of growth kinetics 'phase reentrency' in polymer crystallization. Polymer 39:4561
10. Jacoby P, Bersted BH, Kissel WJ, Smith CE (1986) Studies on the β-crystalline form of isotactic polypropylene. J Polym Sci Polym Phys 24:461
11. Kotek J, Raab M, Baldrian J, Grellmann W (2002) The effect of specific β-nucleation on morphology and mechanical behaviour of isotactic polypropylene. J Appl Polym Sci 85:1174
12. Meille SV, Ferro DR, Brückner S, Lovinger AJ, Padden FJ (1994) Structure of β-isotactic polypropylene: a long-standing structural puzzle. Macromolecules 27:2615
13. Meille SV, Brückner S, Porzio W (1990) γ-Isotactic polypropylene. A structure with nonparallel chain axes. Macromolecules 23:4114
14. Kalay G, Zhong Z, Allan P, Bevis MJ (1996) The occurrence of the γ-phase in injection moulded polypropylene in relation to the processing conditions. Polymer 37:2077
15. Tjong SC, Shen JS, Li RKY (1995) Impact fracture toughness of β-form polypropylene. Scr Metall Mater 33:503
16. Garbarczyk J, Sterzynski T, Paukszta D (1989) Influence of additives on the structure and properties of polymers. 4. Study of phase transition in isotactic polypropylene by synchrotron radiation. Polym Commun 30:153
17. Aboulfaraj M, G'Sell C, Ulrich B, Dahoun A (1995) In situ observation of the plastic deformation of polypropylene spherulites under uniaxial tension and simple shear in the scanning electron microscope. Polymer 36:731
18. Karger-Kocsis J, Varga J (1996) Effects of β-α transformation on the static and dynamic tensile behaviour of isotactic polypropylene. J Appl Polym Sci 62:291
19. Riekel C, Karger-Kocsis J (1999) Structural investigation of the phase transformation in the plastic zone of β-phase isotactic polypropylene by synchrotron radiation microdiffraction. Polymer 40:541
20. Li JX, Cheung WL (1998) On deformation mechanisms of β-polypropylene. 1. Effect of necking on β-phase PP crystals. Polymer 39:6935
21. Li JX, Cheung WL, Chan CM (1999) On deformation mechanisms of β-polypropylene. 2. Changes of lamellar structure caused by tensile loading. Polymer 40:2089
22. Li JX, Cheung WL, Chan CM (1999) On deformation mechanisms of β-polypropylene. 3. Lamellar structures after necking and cold drawing. Polymer 40:3641
23. Cho K, Saheb DN, Yang H, Kang BI, Kim J, Lee S-S (2003) Memory effect of locally ordered α-phase in the melting and phase transformation behaviour of β-isotactic polypropylene. Polymer 44:4053
24. Torre FJ, Cortázar MM, Gómez MÁ, Ellis G, Marco C (2003) Isothermal crystallisation of iPP/Vectra blends by DSC and simultaneous SAXS and WAXS measurement employing synchrotron radiation. Polymer 44:5209
25. Cho K, Saheb DN, Choi J, Yang H (2002) Real time in situ X-ray diffraction studies on the melting memory effect in the crystallization of β-isotactic polypropylene. Polymer 43:1407
26. Kumaraswamy G, Verma RK, Issaian AM, Wang P, Kornfield JA, Yeh F, Hsiao BS, Olley RH (2000) Shear-enhanced crystallization in isotactic polypropylene. Part 2. Analysis of the formation of the oriented 'skin'. Polymer 41:8931
27. Nogales A, Hsiao BS, Somani RH, Srinivas S, Tsou AH, Balta-Calleja FJ, Ezquerra TA (2001) Shear-induced crystallization of isotactic polypropylene with different molecular weight distributions: in situ small- and wide-angle X-ray scattering studies. Polymer 42:5247
28. Hammersley AP, Riekel C (1989) MFIT: Multiple Spectra Fitting Program. Synchrotron Radiat News 2:24
29. Hammersley AP (1997) FIT2D: an introduction and overview. ESRF Internal Rep ESRF97HA02T
30. Jones AT, Aizlewood JM, Beckett DR (1964) Crystalline forms of isotactic polypropylene. Makromol Chem 75:134
31. Chen HB, Karger-Kocsis J, Wu JS, Varger J (2002) Fracture toughness of α- and β-phase polypropylene homopolymers and random- and block-copolymers. Polymer 43:6505
32. Bessell TJ, Hull D, Shortall JB (1975) Effect of polymerization conditions and crystallinity on mechanical properties and fracture of spherulitic nylon-6. J Mater Sci 10:1127
33. Hull D (1999) Fractography. Cambridge University Press, Cambridge
34. Galeski A (2003) Strength and toughness of crystalline polymer systems. Prog Polym Sci 28:1643
35. Varga J (1992) Review: supermolecular structure of isotactic polypropylene. J Mater Sci 27:2557
36. Schneider K, Zafeiropoulos NE, Häußler L, Stamm M (2004) High-throughput screening of the influence of thermal treatments of the mechanical properties of semicrystalline polymers: a case study for iPP. Macromol Rapid Commun 25:355
37. Kinloch AJ, Young RJ (1983) Fracture behaviour of polymers. Elsevier Applied Science, London